DOI: 10.1002/chem.200700472

Increasing the Number of Oxygen Vacancies on TiO_2 by Doping with Iron Increases the Activity of Supported Gold for CO Oxidation

Silvio Carrettin,[a] Yalin Hao,[b] Veronica Aguilar-Guerrero,[b] Bruce C. Gates,[b] Susana Trasobares,[c] Jose J. Calvino,[c] and Avelino Corma*[a]

Abstract: The addition of iron to high-area TiO_2 (Degussa P25, a mixture of anatase and rutile) increases the number of oxygen defect sites that react with O_2 to form peroxide and superoxide species. In the presence of gold nanoclusters on the TiO_2 surface, the superoxide species become highly reactive, and the activity of the supported gold catalyst for CO oxidation is approximately twice that of the most active comparable catalysts described in the literature. Images of the catalyst obtained by scanning transmission electron microscopy combined with spectra of the catalyst measured in the working state (Raman, extended X-ray absorption fine structure, and X-ray absorption near-edge structure) indicate strong interactions of gold with the support and the presence of iron near the interfaces between the gold clusters and the TiO_2 support. The high activity of the catalysts is attributed to the presence of defects in these sites that activate oxygen.

Keywords: gold · heterogeneous catalysis · iron · oxidation · supported catalysts

Introduction

Since Haruta and co-workers demonstrated the high catalytic activity of gold nanoparticles for CO oxidation,[1,2] the field of catalysis by gold has expanded to include a wide range of other reactions, exemplified by H_2O_2 synthesis,[3] selective oxidation of alcohols, including polyols,[4,5] chemically selective reduction of substituted aromatic nitro compounds,[6] carbon–carbon bond formation,[7] hydrocarbon oxidation,[8] and numerous others.

In their review, Bond and Thompson[9] showed that the activity of supported gold catalysts is strongly influenced by the method of catalyst preparation and the pretreatment conditions. The effect of gold particle size is considered to be of paramount importance, but evidence indicates that, in catalytic CO oxidation, the support may also play an important role, either direct or indirect, in determining the activity and selectivity.[1–2,9–16]

An unresolved issue in the chemistry of gold-catalyzed oxidation is the mechanism of oxygen activation and supply, including the nature and location of its adsorption. Various models have been postulated to account for the role of oxygen; according to some authors,[17,18] oxygen adsorption proceeds directly on gold atoms, whereas others[19,20] propose that oxygen adsorption also occurs on the support, in particular at oxygen vacancies[21,22] such as those on semiconductor materials, especially in the proximity of gold particles as a consequence of the Schottky junction.[23]

Mixed oxides have gained importance in several fields related to applied catalysis and energy conversion.[24] They offer opportunities for tuning the material properties to create specific sites that influence catalytic activity. Among the many supports investigated in gold catalysis, TiO_2 has drawn the most attention because of the excellent activities of the catalysts, as reported by numerous groups.[1,25–27] Modification of TiO_2 by doping with various metals has been reported to improve its photocatalytic activity.[28] The beneficial effect of the dopant is to increase the lifetime of the photocatalyst by modification of the electronic properties, by adding oxygen vacancies and changing the TiO_2 structure.[28] Recently, Shou et al.[29] showed that the intro-

[a] Dr. S. Carrettin, Prof. Dr. A. Corma
Instituto de Tecnología Química, UPV-CSIC
Universidad Politécnica de Valencia
Avda. de los Naranjos s/n, 46022 Valencia (Spain)
Fax: (+34) 96-387-7809
E-mail: acorma@itq.upv.es

[b] Y. Hao, V. Aguilar-Guerrero, Prof. Dr. B. C. Gates
Department of Chemical Engineering and Materials Science
University of California Davis
One Shields Ave., Davis, CA 95616 (USA)

[c] Dr. S. Trasobares, Prof. Dr. J. J. Calvino
Universidad de Cádiz, Facultad de Ciencias
APDO. 40, 11510 Puerto Real (Cádiz) (Spain)

duction of iron as a modifier of Au/TiO_2 catalysts increases the activity and stability, but this material did not have appreciable activity at temperatures below 293 K. In related work, Moreau and Bond[30] prepared an iron-doped catalyst that, although it had improved stability in operation in a flow reactor, had an activity that was close to or slightly less than that of unmodified Au/TiO_2.

Here we show that doping of TiO_2 (Degussa P25, a mixture of anatase and rutile) with iron leads to an increase in the fraction of the rutile phase and a higher density of oxygen vacancies, which are involved in the activation of oxygen in CO oxidation catalysis.[31–33] Our results, which include characterization of the catalysts in the functioning state by X-ray absorption near-edge structure (XANES), extended X-ray absorption fine structure (EXAFS), and Raman spectroscopy, combined with conventional testing in a once-through fixed-bed reactor, give evidence for the participation of surface oxygen species in the CO oxidation reaction.

Results and Discussion

XRD and UV/Vis studies of formation of defect sites in iron-doped catalysts: Degussa TiO_2 P25 (80% anatase, 20% rutile) was used to prepare the catalysts described in this work. The introduction of a small amount of Fe^{3+} into the TiO_2 structure leads to replacement of Ti^{4+} with Fe^{3+} and promotes the formation of rutile, which, in principle, can stabilize a larger number of defects than pure anatase.[26] As expected, the XRD pattern of the promoted sample (Figure 1) showed that the ratio of rutile to anatase increased when Fe was introduced. Thus, we expect that substitution of Ti^{4+} by Fe^{3+} occurred in the framework and presumably also led to an increase in the number of surface vacancies.

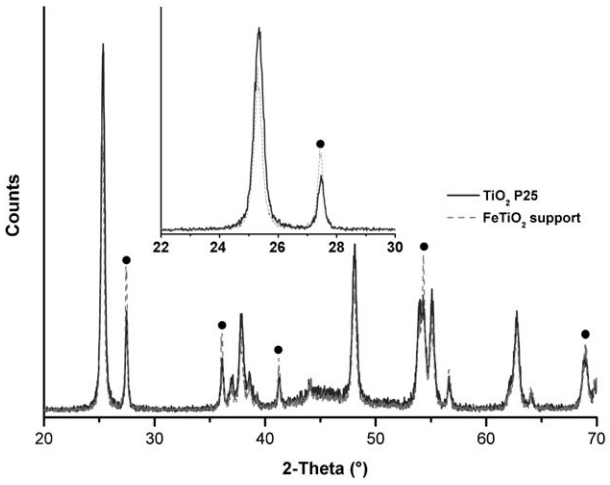

Figure 1. XRD patterns of TiO_2 P25 and Fe-modified TiO_2 P25. (Full circles indicate peaks of the rutile phase).

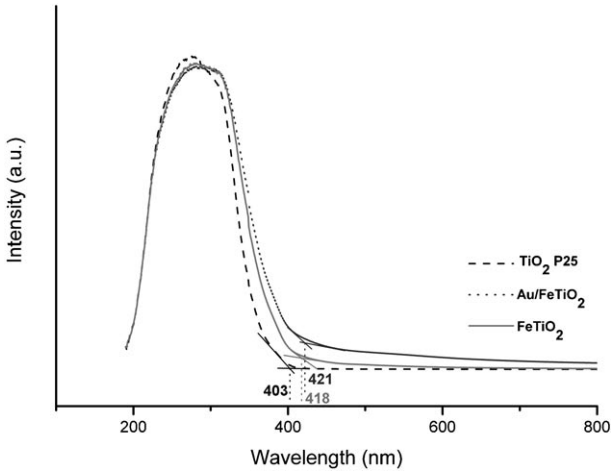

Figure 2. UV/Vis spectra of the supports and the $Au/Fe\text{-}TiO_2$ catalyst.

The UV/Vis spectra (Figure 2) bolster the XRD results: the onset of the band-gap transition (at 418 nm) is red-shifted relative to that of the undoped TiO_2 (403 nm). The shift can be related to the transfer of 3d electrons from Fe^{3+} ions to the conduction band of TiO_2,[34] consistent with the incorporation of Fe^{3+} into the titania matrix. Because a larger red shift was observed when gold was added to the samples (421 nm), we infer that gold further increased the formation of defects.

STEM characterization of iron and gold distributions in $Au/Fe\text{-}TiO_2$: To obtain additional information about the distribution of iron and gold, the catalysts were characterized by scanning transmission electron microscopy (STEM). Both analytical results (energy-dispersive X-ray spectroscopy, X-EDS) and structural information were obtained for the 1.5 wt% $Au/Fe\text{-}TiO_2$ sample. The large difference in atomic number between Au ($Z=79$) and the elements present in the support (Fe, $Z=26$; Ti, $Z=22$) allowed detection with high reliability of the gold nanoparticles in the catalysts in STEM high-angle annular dark field (HAADF) images. These images (Figure 3) show gold particles that are evenly dispersed on the surfaces of the support crystallites, with diameters in the range of 1–50 nm. In contrast, iron appears to be homogeneously distributed over all the support crystallites.

Analysis by STEM X-EDS with a 0.5 nm electron probe gave evidence of only very weak Fe signals representing the support (Figure 4). The aggregation of iron into particles can be ruled out on the basis of the STEM X-EDS data: X-EDS signals indicative of highly dispersed iron were evident, both for support locations not covered by gold clusters and those where gold particles were observed. An implication of these results is that iron was present near the interfaces between the gold particles and the support.

Raman characterization of reactive oxygen species: Defects (oxygen vacancies) in the structures of TiO_2 or CeO_{2-x} can participate in the activation of O_2 by forming peroxides and

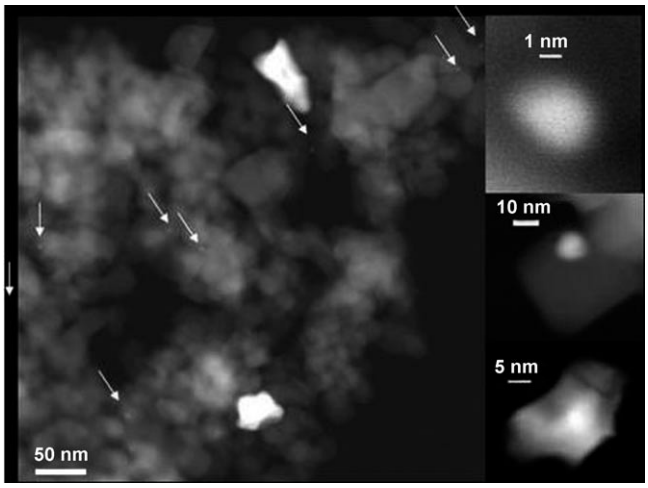

Figure 3. STEM HAADF image of 1.5% Au/Fe-TiO_2 catalyst. Bright spots correspond to Au particles (some of the smaller ones are indicated by arrows). Images on the right illustrate the three characteristic sizes of gold particle observed in this sample.

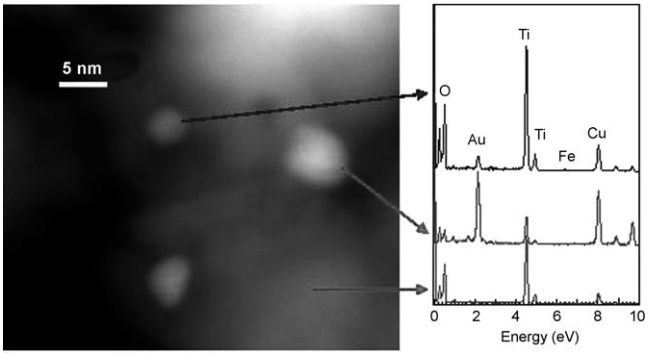

Figure 4. Left: STEM-HAADF image of the 1.5% Au/Fe-TiO_2 catalyst. Right: STEM (0.5 nm probe size) X-EDS spectra recorded at the locations indicated by arrows. Top and middle spectra were obtained for regions covered by gold particles. The bottom spectrum corresponds to an Au-free area. Cu peaks are not from the sample but attributed to the copper grid used to support the sample for STEM measurements.

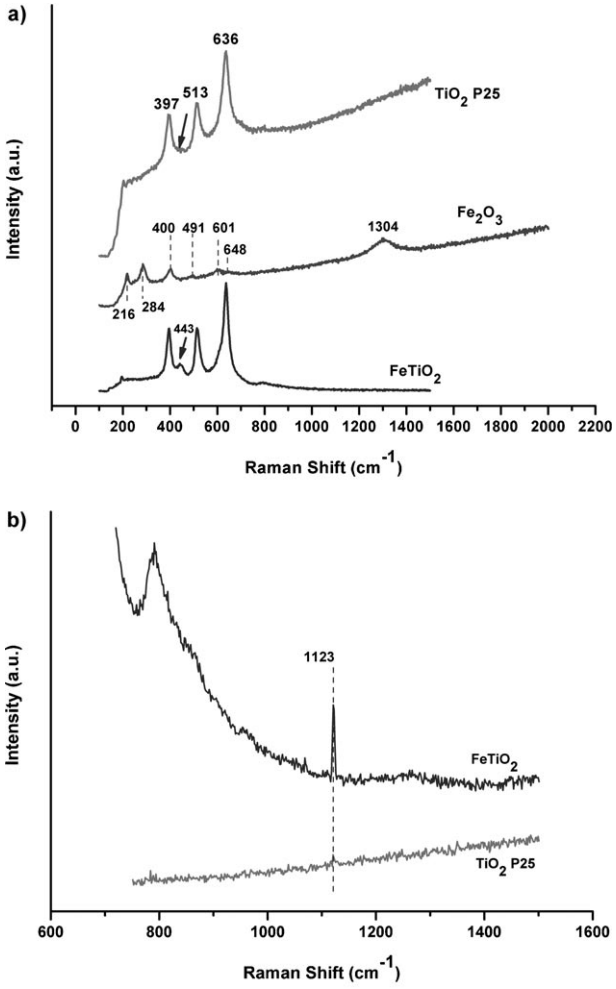

Figure 5. Raman spectra of a) TiO_2 P25, Fe_2O_3, and Fe-modified TiO_2 P25; b) TiO_2 P25 and Fe-modified TiO_2 P25 in the presence of O_2.

superoxides.[28–33] In our case, the presence of reactive oxygen species was confirmed by Raman spectra of the catalyst in the functioning state. Characteristic Raman modes of TiO_2 and Fe_2O_3 are shown in Figure 5a. TiO_2 is characterized by bands at 397, 513, and 636 cm^{-1}, corresponding to B_{1g}, A_{1g}-B_{1g}, and E_g modes representative of anatase; the band observed at 443 cm^{-1} is assigned to the E_g mode of rutile.[35,36] Typically, the rutile phase is also characterized by a band at 612 cm^{-1} (A_{1g} mode), but this is not evident in the spectra of our samples, probably, we infer, because it overlaps with the band at 636 cm^{-1} characteristic of anatase.

The Raman spectrum of Fe_2O_3 includes bands at 216 and 284 cm^{-1}, assigned to A_{1g} modes, and at 400, 491, 601, and 648 cm^{-1}, assigned to E_{1g} vibrational modes of α-Fe_2O_3. The band at 1304 cm^{-1} is assigned to second harmonic vibrations of hematite.[37]

In the presence of O_2, superoxide species are formed on TiO_2 P25, but their density is greater when the TiO_2 is modified with iron, as evidenced by the increased intensity of the band at 1123 cm^{-1} assigned to superoxides (Figure 5b). Raman spectra of the sample in an O_2 atmosphere show that the formation of activated oxygen species is favored on Au/Fe-TiO_2 relative to either Au/TiO_2 or Au/Fe_2O_3 (Figure 6).

The reactivity of the species on the surfaces of the various catalysts was investigated by bringing them into contact with flowing O_2 (30 mL min^{-1}) for 30 min followed by the introduction of a flowing $CO+O_2$ mixture (30 mL min^{-1}) at 253 K and atmospheric pressure. The spectra representing the Au/$FeTiO_2$ catalyst at the beginning and end of the period of CO oxidation catalysis are shown in Figure 7a. The fresh Au/Fe-TiO_2 catalyst was represented by a Raman band at 1122 cm^{-1}, assigned to η^1-superoxide species, and a band at 969 cm^{-1}, assigned to peroxide adspecies at one-electron defect sites.[32] After contacting the sample with $CO+O_2$, the bands at 1122 and 969 cm^{-1} disappeared.

For comparison, the Raman spectrum of Au/TiO_2 includes only a very small contribution attributed to superoxide species (Figure 7b), and the reactivity of this species with CO

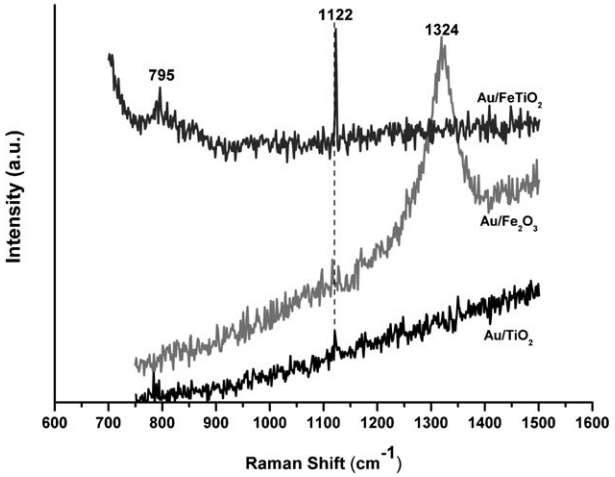

Figure 6. Raman spectra of Au/TiO_2, Au/Fe_2O_3, and $Au/FeTiO_2$ in the presence of oxygen at 253 K (30 mL min^{-1}).

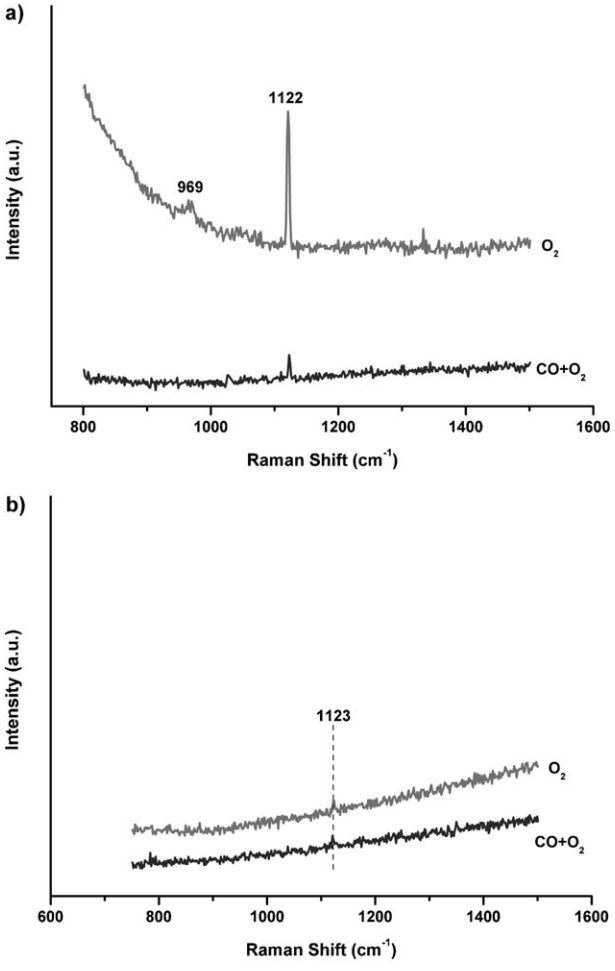

Figure 7. Raman spectra of $Au/FeTiO_2$ (a) and Au/TiO_2 (b) catalysts in O_2 and $CO+O_2$ atmospheres at 253 K.

was shown to be low. In contrast, Au/Fe_2O_3 did not form any detectable peroxide or superoxide species. Thus, the Raman data of the catalysts in reactive atmospheres demonstrate clearly that modification of TiO_2 by addition of iron leads to an increase in the number of surface defects (in particular, oxygen vacancies), which, in the presence of O_2, provide the catalyst with highly reactive surface oxygen species.

XANES and EXAFS characterization of functioning catalyst: All three Au/Fe-TiO_2 samples (with Au loadings of 0.3, 1.5, and 3 wt%) were characterized by XANES and EXAFS spectroscopy. The quality of the EXAFS data of the catalyst with the highest gold loading was good enough to generate reportable analysis results. Characterization was carried out under conditions of CO oxidation catalysis.

The XANES spectra provide qualitative information about the oxidation state of gold in the samples. The intensity of the white line (located at an energy approximately 3–4 eV higher than the Au L_{III} edge) corresponds to the $2p_{3/2}$ to 5d transition; it is proportional to the density of unoccupied states. Gold(III) compounds usually exhibit a high-intensity white line because their d orbitals are only partially occupied. White-line intensities are lower in the XANES spectra of Au^+ compounds and even lower in those of Au^0 compounds. The shape and intensity of other XANES features characteristic of gold compounds, such as those at approximately 15, 25, and 50 eV beyond the Au L_{III} edge, depend on the oxidation state of gold and the ligand environment.

Time-resolved XANES spectra (Figure 8a–c) indicate the presence of cationic gold in each of the three fresh catalysts, as indicated by the white line in the Au L_{III} near-edge region. Among the XANES spectra of the fresh catalysts, that of the sample with the highest gold loading (3 wt%) has the highest white-line intensity.

This result is consistent with the lack of a detectable Au–Au contribution and the presence of an Au–O contribution in the EXAFS spectrum of this sample (Table 1). Two Au–O shells were observed, at 2.03 and at 2.92 Å, with coordination numbers of 2.3 and 0.9, respectively. The EXAFS data also indicate an Au–Ti contribution at 3.16 Å with a coordination number of 0.4 (but the identification of this (weak) contribution is only tentative). Thus, all of these data indicate the presence of cationic gold without detectable zero-valent gold in this sample in the as-prepared state.

The white-line intensities in XANES spectra of the fresh samples incorporating 0.3 and 1.5 wt% Au are lower than that in the XANES spectrum of the fresh Au/Fe-TiO_2 sample containing 3 wt% Au, consistent with lower contents of cationic gold in the former samples. This comparison suggests that these samples initially contained mixtures of cationic and zero-valent gold.

The transient XANES data recorded after the flow of $CO+O_2$ started (Figure 8a–c) show that the cationic gold was rapidly reduced to zero-valent gold under the conditions of catalytic CO oxidation. Evidence for this includes the decline in intensity of the white line and the changes in intensity and shape of the features at 15, 25, and 50 eV beyond the edge. The samples incorporating 0.3 and 1.5 wt% Au were apparently completely reduced and showed features of zero-

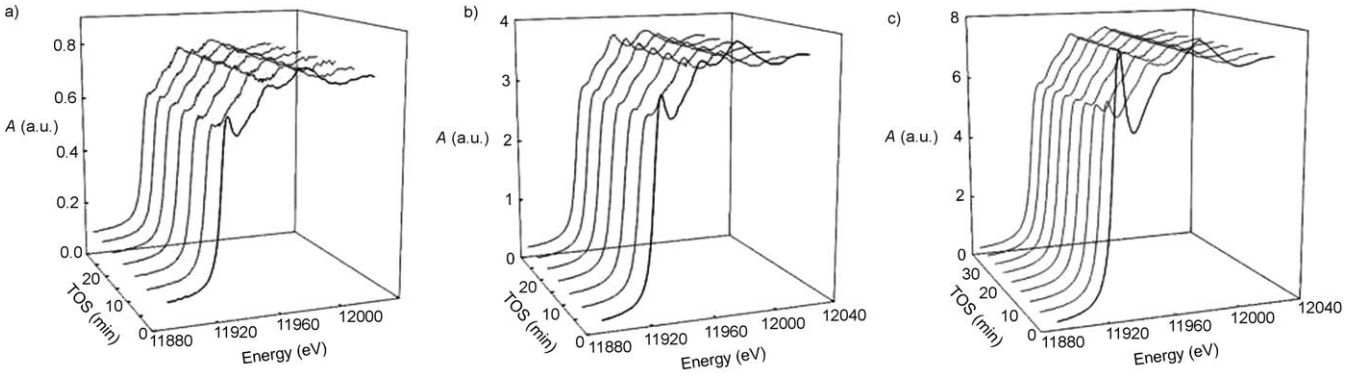

Figure 8. Time-resolved XANES spectra of samples with a) 0.3 %, b) 1.5, and c) 3 % Au during CO oxidation at 298 K. A = normalized absorbance.

Table 1. EXAFS data of 3 % Au/Fe-TiO_2.

Sample treatment	Shell[c]	N	R [Å]	$10^3\Delta\sigma^2$ [Å^2]	E_0 [eV]
before reaction[a]	Au–O_s	2.3	2.03	−0.1	4.0
	Au–O_l	0.9	2.82	−0.8	3.9
	Au–Ti	0.4	3.16	−0.4	−2.7
during reaction[b]	Au–Au	5.4	2.81	8.9	−3.3
	Au–Ti	0.1	3.32	−0.4	−2.4

[a] The k and r ranges for data analysis of this sample were Δk = 3.90–15.06 Å^{-1} and Δr = 1.0–4.0 Å. [b] The k and r ranges for data analysis of this sample were Δk = 3.90–15.24 Å^{-1} and Δr = 1.0–4.0 Å. [c] Subscripts s and l denote short and long, respectively.

valent gold within 5 min on stream. However, it took 15 min on stream to completely reduce the sample incorporating 3 wt % Au, which initially showed features of only cationic gold. Similar observations have been reported for numerous other oxide-supported gold catalysts,[39,40] including TiO_2-supported gold catalysts.[41]

We emphasize 1) that the XANES data characterizing the working catalysts give evidence for zero-valent but not cationic gold in the working catalysts (although cationic gold was present initially), and 2) that these data were obtained at 298 K (whereas the catalysis experiments with the conventional once-through flow reactor were carried out between 253 and 278 K). Thus, the changes observed in the XANES experiments might have taken place more rapidly than in the conventional catalysis experiments. Because of the differences in temperature of the XANES and steady-state catalysis experiments, we infer that the conclusions based on XANES data characterizing the steady state catalysts may not pertain.

The EXAFS data of the catalyst containing 3 wt % Au confirm the presence of zero-valent gold (gold clusters) after the start of the catalytic CO oxidation reaction. These clusters are indicated by an Au–Au contribution that grew in while the sample was in contact with $CO + O_2$; this contribution is characterized by a coordination number of 5.4 (Table 1, corresponding to clusters of approximately 16 Au atoms each, on average, as determined by the model of Jentys[42]).

The growth of the gold clusters during catalytic CO oxidation was accompanied by the disappearance of the short Au–O contribution in the EXAFS spectrum. This result is consistent with XANES evidence for the formation of zero-valent gold and the suggestion that most of the gold was zero-valent for most of the period on stream during catalysis. The EXAFS data of the functioning catalyst also indicate a small Au–Ti contribution, at 3.32 Å, with a coordination number of 0.1 (Table 1). This contribution is evidence of the metal–support interface, but it is too small to allow any confident conclusion about the structure of this interface.

In summary, the EXAFS and XANES data demonstrate the presence of small gold clusters in the working catalyst at steady state, consistent with earlier EXAFS and XANES observations,[38] and they are consistent with the inference that these clusters are part of the catalytically active species.

CO oxidation activity: The data characterizing the catalytic reaction allow comparison of our Au/Fe-TiO_2 catalysts with the Au/TiO_2 and Au/Fe_2O_3 catalysts supplied by the World Gold Council (WGC),[43] which are recommended as standards for reference. Our catalysts containing 1.5 and 3 wt % Au on Fe-TiO_2 have activities significantly higher than those of the reference catalysts at 278 K (Figure 9). Because of its high activity, our Au/Fe-TiO_2 catalyst with an Au loading of 1.5 wt % was tested under conditions similar to those reported by Schüth et al.[27] for various 1 % Au/TiO_2 catalysts (at 253 K). A catalyst with a loading of 1.5 wt % Au was made to be comparable to a reported catalyst.[27]

The catalytic test results show that the 1.5 % Au/TiO_2-Fe catalyst is twice as active per gold atom as the most active Au/TiO_2 catalyst reported by Schüth et al.[27] under similar reaction conditions (Table 2, entries 1 and 5). Our catalyst is also compared in Table 2 with other Au/TiO_2 catalysts reported to be highly active for CO oxidation.[2,20,27] Our data show that the activities of these catalysts were all markedly lower than that of our Fe-doped Au/TiO_2 (Table 2).

The enhanced activity of Au/Fe-TiO_2 can be explained by a positive effect of iron doping, which we infer influenced the activity of the catalyst by increasing the interaction of the gold with the support (as evidenced by STEM) and gen-

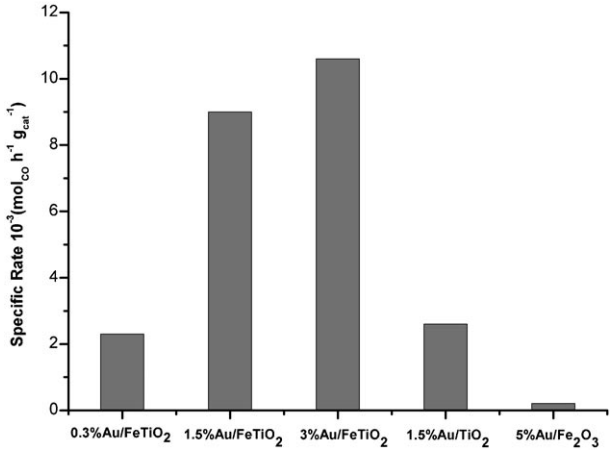

Figure 9. Specific rate of CO oxidation on supported gold catalysts. The reference catalysts 1.5% Au/TiO_2 and 5% Au/Fe_2O_3 were supplied by the World Gold Council.[47] Reaction conditions: molar ratio CO:air:He 0.2:19.8:80, with an inverse space velocity (W/F) of 94 $g_{cat}\,h\,mol_{CO}^{-1}$; reaction temperature 278 K.

Table 2. Comparison of activities of catalysts for CO oxidation at 253 K.

Entry	Catalyst	GHSV [h^{-1}]	Rate 10^{-6} [$mol_{CO}\,g_{cat}^{-1}\,s^{-1}$]	Ref.
1	1% Au/TiO_2	80000	5[a]	[22]
2	3.4% Au/TiO_2	20000	3.5[a]	[1]
3	1% Au/TiO_2	17000	3.7[a]	[20]
4	13.7% Au/TiO_2	40000	5[a]	[21]
5	1.5% $Au/FeTiO_2$	84000	10	this work

[a] The activities for the literature catalysts were calculated from the activity graphs reported by the authors.

erating defects where O_2 can be activated by forming highly reactive oxygen species.

The combination of spectroscopic and catalyst-performance results offers a relatively complete picture of the working catalyst. Modification of the TiO_2 by introduction of a small amount of iron (ca. 0.5 wt%) leads to the substitution of Ti^{4+} ions by Fe^{3+} in the TiO_2 structure and generates oxygen vacancies. The XRD and Raman data show that modification with iron promotes the formation of rutile, which has a higher tolerance for defects than anatase (Figures 1 and 5a)[26] (larger amounts of iron might be expected to lead to the formation of a surplus of oxygen vacancies that would be expected to combine to form extended defect structures similar to crystallographic shear planes[26]). The superior activity of gold supported on iron-modified TiO_2 relative to Au/TiO_2 could then be attributed to the presence of highly reactive oxygen species (specifically, η^1-superoxide and peroxide adspecies) at one-electron defect sites, consistent with the Raman spectra of the working catalyst. These species were not observed on Au/Fe_2O_3 and were present in a much lower density in the unmodified Au/TiO_2 catalyst.

Increasing the gold loading led to an increase in the intensity of the η^1-superoxide Raman band at 1123 cm^{-1}. Thus, a correlation was found between the rate of CO oxidation, the gold loading, and the relative intensity of the bands of the η^1-superoxide species in these catalysts (Figure 10). According to these results, the increased gold loading enhances the number of surface peroxide species and thus results in a higher rate of CO oxidation.

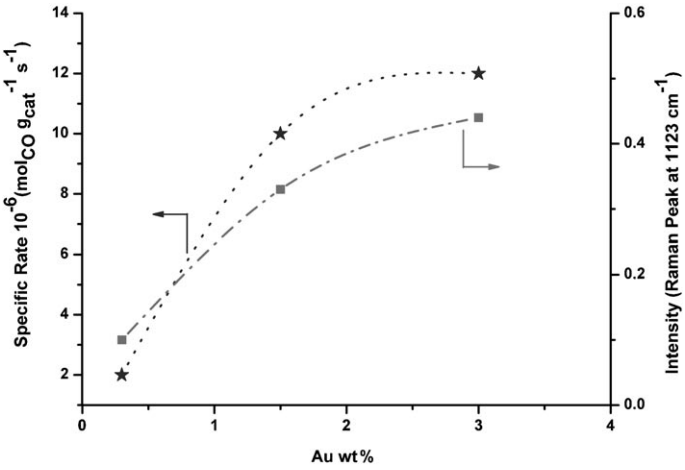

Figure 10. Catalytic activity (stars) and Raman intensity I (squares) of the 1123 cm^{-1} band (η^1-superoxide) as a function of the gold loading at 253 K, GHSV = 84000 h^{-1}.

The EXAFS and XANES data showed the presence of cationic gold in the as-prepared catalyst samples, and these species were largely and rapidly reduced to zero-valent gold under catalytic reaction conditions; the resultant gold clusters were extremely small, and the data are consistent with the suggestion that they were the catalytically active species, or at least part of these species.

The EXAFS results indicate a strong interaction between the gold in these clusters and the support, as evidenced by the Au–O contribution (and tentatively by the Au–Ti contribution). The Au–O contributions beyond the bonding distance (Table 1) indicate nonbonding interactions of the gold clusters with oxygen of the support surface.[33] Earlier work with ceria-supported gold catalysts[33] led to the suggestion that Au–O contributions at longer distances might include Au–peroxide and/or Au–superoxide interactions, but the EXAFS data characterizing the samples reported in this work are not sufficient to support this suggestion.

In summary, our results indicate cooperation between gold and the Fe-TiO_2 support that promotes the formation of reactive oxygen species (Figure 11). We suggest that the CO molecules are adsorbed and activated on the gold clusters, as the oxygen vacancies generated by the presence of Fe^{3+} will activate molecular oxygen by forming superoxide species that interact with the adsorbed CO to form CO_2. The enhanced activity of the catalysts prepared with the iron-modified TiO_2 support is inferred to result from the promoting effect of iron in forming oxygen vacancies at the cluster–support interface, near which reactive intermediate oxygen species are generated.

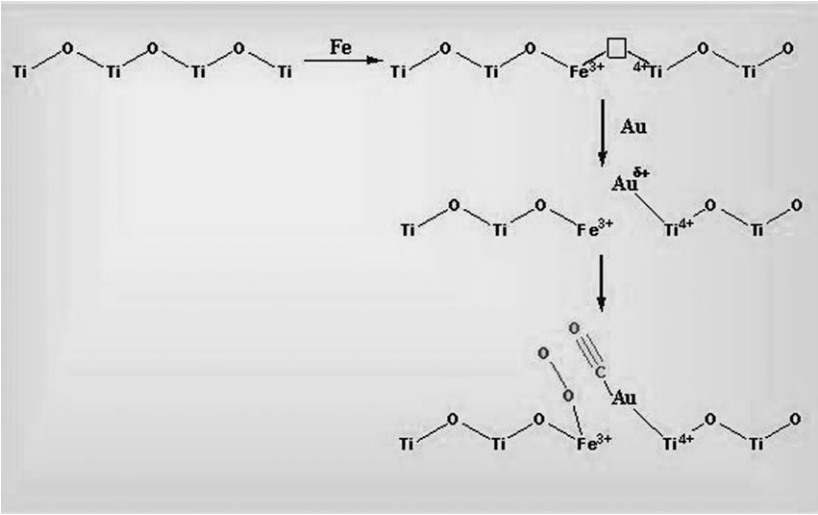

Figure 11. Schematic representation of CO oxidation catalyzed by gold on Fe-TiO_2. CO is adsorbed on the gold, whereas the oxygen is supplied through the support as η^1-superoxide and peroxide adspecies at one-electron defect sites to give CO_2.

Conclusion

The data reported here demonstrate a correlation between the catalytic activity of gold supported on iron-modified TiO_2 and the density of reactive η^1-superoxide and peroxide species at one-electron defect sites on the support. The formation of reactive oxygen species is promoted by the presence of iron cations in the TiO_2 structure. The resulting catalyst has an activity for CO oxidation that in some cases is more than twice those of some of the most active TiO_2-supported gold catalysts yet reported.[2,20–22] The possibility of modifying a support to increase the availability of reactive oxygen species such as peroxides is of quite general interest and may be expected to be useful in the design of novel catalysts with enhanced activity and selectivity for various oxidation reactions.

Experimental Section

Catalyst preparation: Samples of TiO_2 (Degussa P25, 10 g, $S_{BET}=55\ m^2 g$) were impregnated with a solution of 0.1715 g of $Fe(NO_3)_3{\cdot}9H_2O$ (Aldrich, 99.9 % purity) in 10 mL of H_2O (milliQ). The slurry was stirred at 333 K until all the liquid had evaporated, and then the solid was dried at 373 K overnight and calcined at 673 K in a static oven for 5 h. The final Fe content was found to be 0.56 wt % by atomic absorption analysis.

Gold was deposited out from a solution of $HAuCl_4$ (Alfa Aesar), brought to pH 9 by addition of 0.2 M NaOH. The support was added and the pH adjusted to 9; the slurry was stirred at 343 K for 1 h while the pH was kept constant by addition of 0.2 M NaOH. The catalyst was then collected by filtration, washed free of chlorine, and dried overnight in an oven at 373 K.

X-ray diffraction: X-ray diffraction (XRD) patterns were collected by using a Philips X'Pert diffractometer equipped with a graphite monochromator, operating at 40 kV and 45 mA and employing nickel-filtered $Cu_{K\alpha}$ radiation ($\lambda=0.1542$ nm).

UV/Vis spectroscopy: Diffuse-reflectance (DR) UV/Vis spectra were collected with a Cary 5 instrument equipped with a "praying mantis" attachment supplied by Herrick.

STEM: Characterization was carried out by means of *Z*-contrast imaging, generated by high-angle annular dark field (HAADF) scanning transmission electron microscopy (STEM). By using an STEM detector with a large inner radius (a HAADF detector), electrons were collected that were not Bragg-scattered. Thus, the HAADF images show few if any diffraction effects, and their intensity is approximately proportional to Z^2. This imaging technique is excellent for tomographic reconstruction, as it generates strong contrast that has a fully monotonic relationship with thickness.

The sample for examination by STEM was prepared by dispersing the catalyst powder in high-purity ethanol and then allowing a drop of the suspension to evaporate on a holey carbon film supported by a 300-mesh copper grid. Samples were then subjected to chemical microanalysis and annular dark-field imaging in a JEOL JEM-2010F STEM instrument operating at 200 kV. The instrument was also fitted with a system for energy-dispersive X-ray (X-EDS) analysis.

Raman spectroscopy of working catalysts: Raman spectra were collected with a Renishaw inVia Raman spectrometer equipped with a Leica DMLM microscope and a 514 nm Ar^+ ion laser as excitation source. A ×50 objective of 8 mm optical length was used to focus the depolarized laser beam on a spot of about 2 μm in diameter, and the laser power at the sample was 16.0 mW. Raman scattering was measured with a CCD array detector in the 100–2000 cm^{-1} spectral region with a resolution of 2 cm^{-1}. Each reported spectrum is the average of 20 scans, each with an exposure time of 10 s.

Catalytic CO oxidation was conducted with samples in an in situ cell (Linkam Scientific, THMS 600). Gases were introduced into the cell by mass flow controllers at a total gas flow rate of 50 mL min^{-1}; experiments were carried out at temperatures between 298 and 133 K with feeds of O_2, He, and a reaction mixture containing 2.0 vol % CO and 1.0 vol % O_2, balance He.

XANES and EXAFS spectroscopy: The experiments were done at beamline 2-3 at the Stanford Synchrotron Radiation Laboratory. A germanium 13-element detector was used to record the fluorescence signals. The cell enabled the collection of data with the sample in the presence of flowing CO and O_2 under catalytic reaction conditions.[47] Before the powder sample was loaded into the cell, it was weighed and mixed with inert boron nitride powder. The loaded cell was then aligned at the beamline, and XANES and EXAFS spectra were recorded. All the experiments were conducted with the samples at room temperature (ca. 298 K).

We first recorded six EXAFS spectra of each sample in flowing helium (100 mL(NTP) min^{-1}). Then, after the catalytic reaction started as the feed of $CO+O_2$, (1.5 vol % CO and 1.5 vol % O_2, balance He, total flow rate = 100 mL (NPT) min^{-1}) was introduced into the reactor/cell, XANES spectra were recorded repeatedly for at least half an hour to ensure that the spectrum was not changing. Then a sequence of another six EXAFS spectra was recorded for the sample under catalytic reaction conditions.

The EXAFS data were analyzed with a difference file technique by using the software XDAP.[48,49] No attempt was made to account for the small atomic X-ray fine structure (as would be indicated by data obtained at low values of *r*, the distance from the absorber atom, Au), and the standard background subtraction technique was applied. Experimentally determined reference files prepared from EXAFS data representing materi-

Table 3. Crystallographic data of reference compounds and Fourier transform ranges used in the EXAFS analysis.[a]

Reference compound	Shell	Crystallographic data			Fourier transform	
		N	R [Å]	Ref.	Δk [Å^{-1}]	Δr [Å]
Au	Au–Au	12	2.88	[44]	1.00–20.00	0.00–8.00
$Na_2[Pt(OH)_6]$	Pt–O (Au–O)	6	2.05	[45]	2.67–15.69	0.00–2.10
AuTi	Au–Ti	12	2.90	[46]	1.00–20.00	0.00–8.00

[a] N is coordination number, R is distance between absorber and backscatterer atoms, and Δk and Δr are the ranges used in the Fourier transformation.

als of known structure[45] and theoretically determined reference files calculated with the software FEFF 7.0[50] were used in the analysis (Table 3).

The quality of the fluorescence EXAFS data of the sample with the highest gold loading (3 wt %) was high; however, the technique did not lead to reportable data for the samples with lower gold loadings. Thus, in the following paragraphs we describe the EXAFS data fitting only for the sample with the highest gold loading.

The number of parameters used in fitting the data to each candidate model was justified statistically by the Nyquist theorem:[51] $n=(2\Delta k\Delta r/\pi)+1$, where Δk and Δr, respectively, are the ranges in k and r used in the data fitting (k is the photoelectron wave vector). The fitting was carried out with a maximum of 12 free parameters (corresponding to three absorber/backscatterer contributions), less than the value of n determined by the Nyquist theorem. Iterative fitting was carried out until good agreement was obtained between the calculated k^0-, k^1-, and k^3-weighted data and the postulated model. The estimated accuracies in determination of EXAFS parameters of the Au–Au and Au–O contributions are as follows: coordination number N, ±20 %; distance R, ±1 %; Debye–Waller factor relative to the reference material $\Delta\sigma^2$, ±30 %; inner potential correction (ΔE_0), ±10 %.[52]

CO oxidation catalysis: CO oxidation was carried out at atmospheric pressure in a standard once-through, nearly isothermal, tubular, packed-bed flow reactor (9 mm i.d.). The total feed flow rate to the reactor was 100 mL(NTP) min^{-1} with a molar ratio of CO:air:He of 0.2:19.8:80.0 and an inverse space velocity of 94.0 $g_{cat}\,h\,mol_{CO}^{-1}$.

Tests for comparison of our catalyst and literature catalysts in terms of performance for CO oxidation were carried out at 253 K under the following conditions: feed, 2 % CO/1 % O_2/He 70 mL min^{-1}; catalyst, 1.5 % Au/Fe-TiO_2; catalyst mass, 0.05 g; inverse space velocity W/F, where W is the catalyst mass and F the molar flow rate of CO, 13.3 $g_{cat}\,h\,mol_{CO}^{-1}$ (gas hourly space velocity (GHSV) of 84 000 h^{-1}). Conversions were determined by gas chromatographic analysis of the product stream, with an accuracy of about ±5 %. The on-line gas chromatograph (Varian Star 3400 CX) was equipped for switching between columns (Porapak and molecular sieves) in combination with a thermal conductivity detector. The catalytic data were collected under steady-state conditions.

Acknowledgements

We thank the Auricat European Union network (HPRN-CT-2002-00174) for financial support, Johnson Matthey plc (Alfa Aesar) for the loan of the gold precursor and Degussa AG for providing a sample of TiO_2 P25. We also acknowledge support by the U.S. Department of Energy, Office of Basic Energy Sciences (DE-FG02-04ER15513) and the Stanford Synchrotron Radiation Laboratory.

[1] M. Haruta, T. Kobayashi, H. Sano, N. Yamada, *Chem. Lett.* **1987**, 405–408.
[2] M. Haruta, N. Yamada, T. Kobayashi, S. Iijima, *J. Catal.* **1989**, *115*, 301–309.
[3] P. Landon, P. J. Collier, A. J. Papworth, C. J. Kiely, G. J. Hutchings, *Chem. Commun.* **2002**, 2058–2059.
[4] S. Biella, L. Prati, M. Rossi, *J. Catal.* **2002**, *206*, 242–247.
[5] a) S. Carrettin, P. McMorn, P. Johnston, K. Griffin, G. J. Hutchings, *Chem. Commun.* **2002**, 696–697; b) A. Abad, P. Concepcion, A. Corma, H. Garcia, *Angew. Chem.* **2005**, *117*, 4134–4137; *Angew. Chem. Int. Ed.* **2005**, *44*, 4066–4069; .
[6] A. Corma, P. Serna, *Science* **2006**, *313*, 332–334.
[7] S. Carrettin, J. Guzman, A. Corma, *Angew. Chem.* **2005**, *117*, 2282–2285; *Angew. Chem. Int. Ed.* **2005**, *44*, 2242–2245; .
[8] M. D. Hughes, Yi-Jun Xu, P. Jenkins, P. McMorn, P. Landon, D. I. Enache, A. F. Carley, G. A. Attard, G. J. Hutchings, F. King, E. Hugh Stitt, P. Johnston, K. Griffin, C. J. Kiely, *Nature* **2005**, *437*, 1132–1135.
[9] G. C. Bond, D. T. Thompson, Catal. *Rev. Sci. Eng.* **1999**, *41*, 319–388.
[10] a) S. Tsubota, T. Nakamura, K. Tanaka, M. Haruta, *Catal. Lett.* **1998**, *56*, 131–135; b) M. Haruta, S. Tsubota, T. Kobayashi, H. Kageyama, M. J. Genet, B. Delmon, *J. Catal.* **1993**, *144*, 175–192; c) F. Boccuzzi, A. Chiorino, M. Tsubota, M. Haruta, *Catal. Lett.* **1994**, *29*, 225–234; d) D. A. H. Cunningham, W. Vogel, H. Kageyama, S. Tsubota, M. Haruta, *J. Catal.* **1998**, *177*, 1–10.
[11] a) J. Guzman, B. C. Gates, *J. Phys. Chem. B* **2002**, *106*, 7659–7665; b) J. Guzman, B. C. Gates, *J. Am. Chem. Soc.* **2004**, *126*, 2672–2673.
[12] Q. Fu, H. Saltsburg, M. Flytzani-Stephanopoulos, *Science* **2003**, *301*, 935–938.
[13] M. S. Chen, D. W. Goodman, *Science* **2004**, *306*, 252–255.
[14] M. Haruta, *CATTECH* **2002**, *6*, 102–115.
[15] S. Carrettin, P. Concepcion, A. Corma, J. M. Lopez Nieto, V. F. Puntes, *Angew. Chem.* **2004**, *116*, 2592–2594; *Angew. Chem. Int. Ed.* **2004**, *43*, 2538–2540; .
[16] J. Guzman, A. Corma, *Chem. Commun.* **2005**, 743–745.
[17] M. Haruta, *Catal. Surv. Jpn.* **1997**, *1*, 61–73.
[18] M. Valden, S. Pak, X. Lai, D. W. Goodman, *Catal. Lett.* **1998**, *56*, 7–10.
[19] J. D. Grunwaldt, A. Baiker, *J. Phys. Chem. B* **1999**, *103*, 1002–1012.
[20] A. I. Kozlov, A. P. Kozlova, H. Liu, Y. Ywasawa, *Appl. Catal. A* **1999**, *182*, 9–28.
[21] H. Liu, A. I. Kozlov, A. P. Kozlova, T. Shido, K. Asakura, Y. Iwasawa, *J. Catal.* **1999**, *185*, 252–264.
[22] H. Liu, A. I. Kozlov, A. P. Kozlova, T. Shido, Y. Iwasawa, *Phys. Chem. Chem. Phys.* **1999**, *1*, 2851–2860.
[23] J. C. Frost, *Nature* **1988**, *334*, 577–580.
[24] J. Larmine, A. Dicks, *Fuel Cell Systems Explained*, Wiley-VCH, Weinheim, **2000**.
[25] F. Moreau, G. C. Bond, A. O. Taylor, *Chem. Commun.* **2004**, 1642–1643.
[26] V. Schwartz, D. R. Mullins, W. Yan, B. Chen, S. Dai, S. H. Overbury, *J. Phys. Chem. B* **2004**, *108*, 15782–15790.
[27] M. Comotti, Wen-Cui Li, B. Spliethoff, F. Schüth, *J. Am. Chem. Soc.* **2006**, *128*, 917–924.
[28] M. R. Hoffmann, S. T. Martin, W. Y. Choi, D. W. Bahnemann, *Chem. Rev.* **1995**, *95*, 69–96.
[29] M. Shou, H. Takekawa, D-Y Ju, T. Hagiwara, Da-ling Lu, Ken-ichi Tanaka, *Catal. Lett.* **2006**, *108*, 119–124.
[30] F. Moreau, G. C. Bond, *Catal. Today* **2006**, *114*, 362–368.
[31] X. H. Wang, J.-G. Li, H. Kamiyama, M. Katada, N. Ohashi, Y. Moriyoshi, T. Ishigaki, *J. Am. Chem. Soc.* **2005**, *127*, 10982–10990.
[32] J. Guzman, S. Carrettin, A. Corma, *J. Am. Chem. Soc.* **2005**, *127*, 3286–3287.
[33] J. Guzman, S. Carrettin, J. C. Fierro-Gonzalez, Y. Hao, B. C. Gates, A. Corma, *Angew. Chem.* **2005**, *117*, 4856–4859; *Angew. Chem. Int. Ed.* **2005**, *44*, 4778–4781; .
[34] A. Kumbhar, G. Chumanov, *J. Nanopart. Res.* **2005**, *7*, 489–498.

[35] T. Ohsaka, F. Izumi, Y. Fujiki, *J. Raman Spectrosc.* **1978**, *7*, 321–324.
[36] S. P. S. Porto, P. A. Fleury, T. C. Damen, *Phys. Rev.* **1967**, *154*, 522–526.
[37] D. Bersani, P. P. Lottici, A. Montenero, *J. Raman Spectrosc.* **1999**, *30*, 355–360.
[38] J. T. Calla, R. J. Davis, *J. Phys. Chem. B* **2005**, *109*, 2307–2314.
[39] C. K. Costello, J. Guzman, J. H. Yang, Y. M. Wang, M. C. Hung, B. C. Gates, H. H. Kung, *J. Phys. Chem. B* **2004**, *108*, 12529–12536.
[40] J. Guzman, B. C. Gates, *J. Phys. Chem. B* **2002**, *106*, 7659–7665.
[41] J. Guzman, S. Kuba, J. C. Fierro-Gonzalez, B. C. Gates, *Catal. Lett.* **2004**, *95*, 77–86.
[42] A. Jentys, *Phys. Chem. Chem. Phys.* **1999**, *1*, 4059–4063.
[43] http://www.gold.org/discover/sci_indu/gold_catalysts/refcat.html
[44] R. W. G. Wycoff, *Crystal Structures, Vol. 1*, 2nd ed., Wiley, New York, **1963**, p. 10.
[45] M. Trömel, E. D. Lupprich, *Z. Anorg. Allg. Chem.* **1975**, *414*, 160–168.
[46] P. Villars, L. D. Calvert, *Pearson's Handbook of Crystallographic Data for Intermetallic Phases, Vol. 1,* ASM International, Materials Park, OH, **1991**, p. 653.
[47] J. F. Odzak, A. M. Argo, F. S. Lai, B. C. Gates, K. Pandya, L. Feraria, *Rev. Sci. Instrum.* **2001**, *72*, 3943–3945.
[48] D. C. Koningsberger, B. L. Mojet, G. E. Dorsen, D. E. Ramaker, *Top.Catal.* **2000**, *10*, 143–155.
[49] M. Vaarkamp, J. C. Linders, D. C. Koningsberger, *Physica B+C* **1995**, *209*, 159–160.
[50] A. L. Ankudinov, J. J. Rehr, *Phys. Rev. B* **1997**, *56*,
[51] E. A. Stern, *Phys. Rev. B* **1993**, *48*, 9825–9827.
[52] O. Alexeev, B. C. Gates, *Top. Catal.* **2000**, *10*, 273–293.

Received: March 27, 2007
Published online: July 4, 2007

